ELSEVIER

NeuroImage

www.elsevier.com/locate/ynimg
NeuroImage 23 (2004) 454–461

Improved delineation of brain tumors: an automated method for segmentation based on pathologic changes of ^{1}H-MRSI metabolites in gliomas

Andreas Stadlbauer,[a,b] Ewald Moser,[a,c,*] Stephan Gruber,[b] Rolf Buslei,[d] Christopher Nimsky,[a] Rudolf Fahlbusch,[a] and Oliver Ganslandt[a]

[a]*Department of Neurosurgery, Neurocenter, University of Erlangen-Nuremberg, Erlangen, Germany*
[b]*NMR Group, Department of Medical Physics, Medical University of Vienna, Vienna, Austria*
[c]*Department of Radiodiagnostics, General Hospital of Vienna, Vienna, Austria*
[d]*Department of Neuropathology, University of Erlangen-Nuremberg, Erlangen, Germany*

Received 19 August 2003; revised 13 May 2004; accepted 11 June 2004
Available online 8 September 2004

In this study, we developed a method to improve the delineation of intrinsic brain tumors based on the changes in metabolism due to tumor infiltration. Proton magnetic resonance spectroscopic imaging (^{1}H-MRSI) with a nominal voxel size of 0.45 cm^{3} was used to investigate the spatial distribution of choline-containing compounds (Cho), creatine (Cr) and *N*-acetyl-aspartate (NAA) in brain tumors and normal brain. Ten patients with untreated gliomas were examined on a 1.5 T clinical scanner using a MRSI sequence with PRESS volume preselection. Metabolic maps of Cho, Cr, NAA and Cho/NAA ratios were calculated. Tumors were automatically segmented in the Cho/NAA images based on the assumption of Gaussian distribution of Cho/NAA values in normal brain using a limit for normal brain tissue of the mean + three times the standard deviation. Based on this threshold, an area was calculated which was delineated as pathologic tissue. This area was then compared to areas of hyperintense signal caused by the tumor in T2-weighted MRI, which were determined by a region growing algorithm in combination with visual inspection by two experienced clinicians. The area that was abnormal on ^{1}H-MRSI exceeded the area delineated via T2 signal changes in the tumor (mean difference 24%) in all cases. For verification of higher sensitivity of our spectroscopic imaging strategy we developed a method for coregistration of MRI and MRSI data sets. Integration of the biochemical information into a frameless stereotactic system allowed biopsy sampling from the brain areas that showed normal T2-weighted signal but abnormal ^{1}H-MRSI changes. The histological findings showed tumor infiltration ranging from about 4–17% in areas differentiated from normal tissue by ^{1}H-MRSI only. We conclude that high spatial resolution ^{1}H-MRSI (nominal voxel size = 0.45 cm^{3}) in combination with our segmentation algorithm can improve delineation of tumor borders compared to routine MRI tumor diagnosis.

Keywords: Brain tumor; MRI; Proton magnetic resonance spectroscopic imaging; High resolution; Segmentation

Introduction

In conventional MRI it is often difficult to delineate the heterogeneous structure of gliomas. Even the current methods of choice, T2-weighted MRI and contrast-enhanced MRI as a technique for visualizing regions where the blood-brain barrier is damaged, are not specific for tumors and can result in ambiguous or misleading results (Dowling et al., 2001; Kondziolka et al., 1993). Establishing the position and the extent of the border zone between tumor and normal brain tissue is one of the major problems in therapy planning. Proton magnetic resonance spectroscopic imaging (^{1}H-MRSI) is a noninvasive tool for investigating the spatial distribution of metabolic changes in brain lesions. Calculation of metabolic maps by integrating the peak area of a metabolite of interest for each voxel is a common method to allow visualization of these changes (Luyten et al., 1990; van Der Veen et al., 2000). Several studies have reported increased levels of choline-containing compounds (Cho) and a reduction in signal intensity of the *N*-acetyl-aspartate (NAA) and creatine (Cr) in brain tumors (Frahm et al., 1991; Majos et al., 2002; Negendank et al., 1996; Ott et al., 1993; Peeling and Sutherland, 1992). Choline-containing compounds are composed of choline, phosphocholine and glycerophosphocholine. The signal of these metabolites is often elevated in the presence of

* Corresponding author. Institut fuer Medizinische Physik, Medizinische Universitaet Wien, Waehringerstrasse 13, A-1090 Vienna, Austria. Fax: +43 1 4277 9607.
E-mail address: ewald.moser@meduniwien.ac.at (E. Moser).
Available online on ScienceDirect (www.sciencedirect.com.)

1053-8119/$ - see front matter © 2004 Elsevier Inc. All rights reserved.
doi:10.1016/j.neuroimage.2004.06.022

tumorous tissue which is thought to be due to increased membrane synthesis in rapidly dividing tumor cells (Michaelis et al., 1993; Miller, 1991).

NAA is regarded as a neuronal marker mainly contained within neurons (Urenjak et al., 1993). tCr, as signal from both creatine and phosphocreatine, plays a role in tissue energy metabolism (Kemp, 2000) and is reduced in astrocytomas, but the implication of this decrease on tumor metabolism is not clear. The range of Cho increase and NAA decrease is compatible with the range of tumor infiltration (Croteau et al., 2001; Dowling et al., 2001). In principle, metabolic maps of NAA and Cho allow the differentiation of necrosis, solid tumor and varying degrees of tumor infiltration as well as tissue edema. With standard spectroscopic imaging techniques at 1.5 T, that is, nominal spatial resolution of about 1 cm^3 or bigger, the differentiation between tumor and normal or edematous brain tissue, however, is not sufficient, especially for the delineation of the tumor infiltration zone. Pathologic changes within a comparatively small volume cannot be detected with standard low-resolution spectroscopic imaging due to partial volume effects.

In this study, we increased the spatial resolution in spectroscopic imaging to a value comparable with the resolution of the frameless stereotactic system used (Steinmeier et al., 2000). Metabolic maps of Cho and NAA were used for computing Cho/NAA ratio images to improve the contrast between apparently normal tissue and tumor. We developed software to achieve automated segmentation of the tumor including the infiltration zone in this ratio map based on the assumption of Gaussian distribution for the Cho/NAA values in normal brain matter. The resulting spectroscopic image of the segmented tumor was used to calculate the area of pathologic brain metabolism due to the lesion. Comparison with the hyperintense area of routine T2w MRI showed higher sensitivity of our strategy of high-resolution MRSI in combination with an automated segmentation algorithm. This result was confirmed with biopsies obtained from the area which has normal signal in the T2w MRIs but abnormally high Cho/NAA in the metabolic maps. To achieve this and to allow integration of biochemical information in a frameless stereotactic system it was necessary to develop a method for coregistration of MRI and MRSI data sets.

Materials and methods

Patients and control subjects

Ten patients (six male, four female, 40 ± 11 years old), all with untreated supratentorial gliomas (WHO grades II and III) were examined in a separate session after routine MRI. This consisted of (a) an axial turbo spin echo (TSE) sequence (T2-weighted, 5-mm slices, TR/TE 4000/98 ms), (b) an axial fluid-attenuated inversion recovery (FLAIR) sequence (5-mm slices, TR/TE 10000/103 ms), and (c) pregadolinium and postgadolinium contrast enhanced coronal gradient echo (GE) sequences (T1-weighted, 5-mm slices, TR/TE 430/12 and 525/17 ms, respectively). Table 1 summarizes tumor type and locations. The reason why no glioblastoma patients were included in this study is that in these tumors very large tumor cell infiltration occurs (sometimes even into the contralateral hemisphere) and therefore no radical surgical approach is possible. Our purpose was to develop an imaging modality to improve the delineation of brain tumors that allows a more radical resection.

Table 1
Grade and location of the 10 brain tumors investigated

Patient no. (age/gender)	Tumor type	WHO grade	Tumor location
1 (49/m)	astrocytoma	II	frontal
2 (21/f)	astrocytoma	II	frontal
3 (33/f)	astrocytoma	II	frontal
4 (56/m)	oligodendroglioma	III	frontal
5 (38/m)	oligoastrocytoma	III	precentral
6 (43/f)	astrocytoma	II	frontal
7 (33/m)	oligoastrocytoma	III	temporo-occipital
8 (46/m)	astrocytoma	III	frontotemporal
9 (34/m)	astrocytoma	III	parietal
10 (53/f)	oligoastrocytoma	III	frontal

Note. All tumors were diagnosed by histopathologic analysis of biopsy samples according to the WHO classification of tumors of the central nervous system. Age in years, f = female, m = male.

This is only achievable in WHO grades I–III tumors and may lead to a higher survival rate. Additionally, an age- and sex-matched control group of 10 healthy volunteers was examined for validation of the segmentation method.

MRI and MRSI acquisition

All studies were performed on a 1.5 T clinical whole body scanner (MAGNETOM Sonata, Siemens Erlangen, Germany) equipped with the standard head coil. In each MRSI session a localization scan and an axial spin echo (SE) sequence (T1-weighted) were acquired for MRSI excitation volume location. The T1w SE sequence was used for matching spectroscopic images to an anatomic three-dimensional magnetic resonance image set (Stadlbauer et al., 2004). The parameters were TR/TE 500/15 ms, 256 × 256 matrix size, 16 × 16 cm FOV, 20 slices with no gap and a slice thickness of 2 mm. The MRSI sequence was performed within the same MRI session immediately afterwards. The MRSI slab with Point-RESolved Spectroscopy (PRESS) volume preselection was aligned precisely to a selected SE slice by copying and pasting the image position. Water suppression was achieved using three CHEmical Shift Selective (CHESS) pulses before the PRESS excitation. The MRSI parameters were TR/TE 1600/135 ms, 24 × 24 circular phase-encoding scheme across a 16 × 16 cm FOV, slice thickness 10 mm, 50% Hamming-filter and 2 NEX, spectral width 1000 Hz and 1024 complex points acquisition size. The total spectroscopic data acquisition time was less than 13 min. The nominal voxel size was 0.67 × 0.67 × 1.00 cm^3 (approximately 0.45 cm^3 resolution). After zero-filling to 32 × 32 matrix size the nominal volume of a voxel was 0.25 cm^3. Taking into account the effect of the applied k-space filter (50% Hamming) on the full-width-at-half-maximum (FWHM) the estimated voxel size was approximately 0.5 cm^3 (Vikhoff-Baaz et al., 2001).

The PRESS excitation volume was positioned to exclude lipids of the skull and subcutaneous fat. While examining patients we covered the whole or at least the bulk of the tumor and as much apparently normal brain tissue as possible.

In a single session 1 day before biopsy sampling a three-dimensional anatomic magnetization prepared rapid acquisition gradient echo (MPRAGE) sequence was performed with the following parameters: TR/TE 2020/4.38 ms, 25 × 25 cm FOV, 1 mm isotropic and 160 slices. This MPRAGE study was used for frameless stereotaxis. For registration in a frameless stereotactic

system (VectorVisionSky, BrainLab, Heimstetten, Germany) 6–8 adhesive skin fiducials were positioned in a scattered pattern on the head surface before imaging.

MRSI data analysis

Zero-filling to 32 × 32 matrix size and 2D spatial Fourier transformation was performed with the manufacturer's data-processing software (syngo MR 2002A). MRSI raw data sets were processed with the freely available reconstruction program csx (for Linux), obtained from PB Barker (Baltimore, USA). Spectroscopic imaging data were exponentially filtered with a line broadening factor of 3 Hz, zero filled to 2048 data points and Fourier transformed with respect to the spectral dimension. To remove the residual water peak we used a high-pass convolution filter (50 Hz stop band) (Jacobs et al., 2001). Magnitude spectra were calculated, the position of NAA was set to 2.02 ppm and a susceptibility correction was applied to correct for voxel-to-voxel frequency shifts. The susceptibility correction was based on finding the frequency of the same resonance peak common to all the spectra. The peak areas for Cho, Cr and NAA were calculated by integration over the frequency range of 3.34–3.14, 3.14–2.94, and 2.22–1.82 ppm, respectively. Smooth linear interpolation to a 256 × 256 matrix resulted in the metabolic maps (Figs. 1A and B). Cho and NAA images were used to calculate a map of Cho/NAA ratios (Fig. 1C).

Our assumptions were (1) the values for Cho/NAA in normal brain follow a Gaussian distribution, and (2) those for the tumor, including the border zone, are significantly increased. These assumptions represent the basis on which our tumor segmentation procedure was developed. We determined a "healthy region" of predominantly white matter on the contralateral side and at a sufficient distance from the lesion according to the Cho/NAA ratio map (red rectangle in Figs. 2A and B). The selected region had to contain a sufficient amount of Cho/NAA values to allow statistical evaluation and to test our assumption of a Gaussian distribution of the Cho/NAA values in the normal brain. The size of the selected region was not related to the size of the tumor but rather chosen to be larger (or at least equal). The characteristics of Gaussian distribution are unimodal, symmetric and mean = median = modal value. Both of the first properties were checked by inspection of the histogram (Fig. 2C), the latter by calculation and comparison of the three characteristic parameters for the Cho/NAA values of the selected region. The test for Gaussian distribution given by David et al. (1954) was additionally performed. In case of a Gaussian distribution there is a relationship between the proportion of cases (here amount of Cho/NAA values) in between an interval of the mean ± n times standard deviation (SD, n = 1, 2, 3,. . .).

For known mean and SD of the Cho/NAA values this means for the Gaussian distributed Cho/Naa values in the normal brain: 68.3% of all Cho/NAA values are contained in an interval of mean ± 1 SD, 95.4% of all Cho/NAA values are contained in an interval of mean ± 2 SD, 99.7% of all Cho/NAA values are contained in an interval of mean ± 3 SD and so on. To perform segmentation of the MRSI data the mean and the standard deviation of the Cho/NAA ratios were calculated for the selected region in the map and

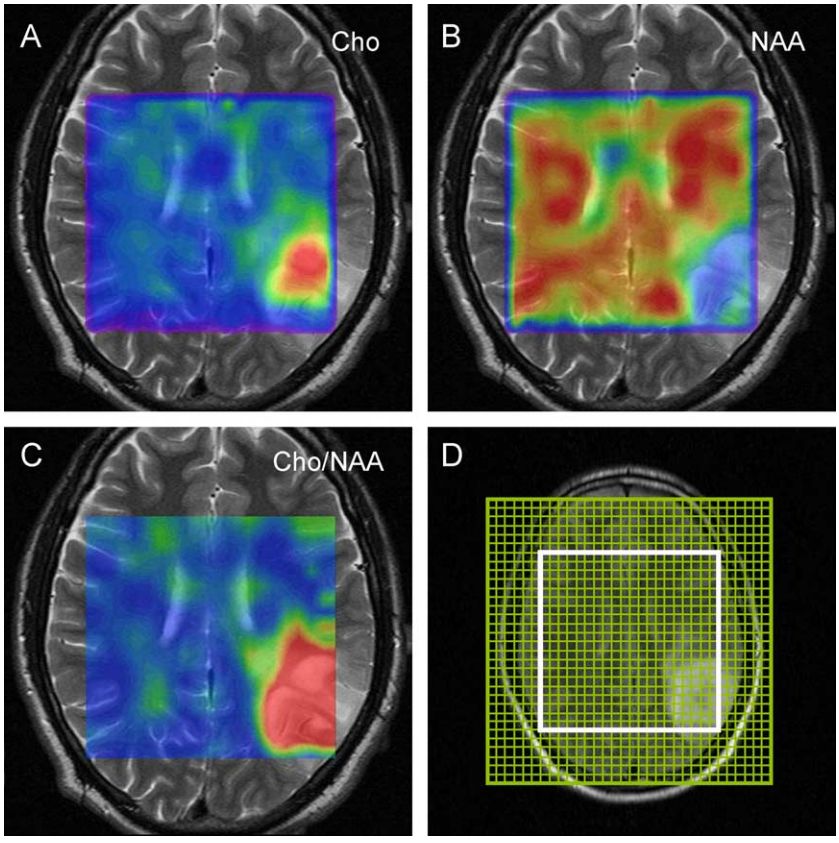

Fig. 1. Spectroscopic images of patient no. 9 with an astrocytoma (WHO grade III), color-coded and overlaid on T2w MRIs. Metabolic map of Cho (A) and NAA (B). (C) Map of the Cho/NAA ratios. (D) Anatomical reference (T2w) overlaid with the CSI grid (green) and the VOI (PRESS box, white rectangle). Color code: violet = minimum, red = maximum.

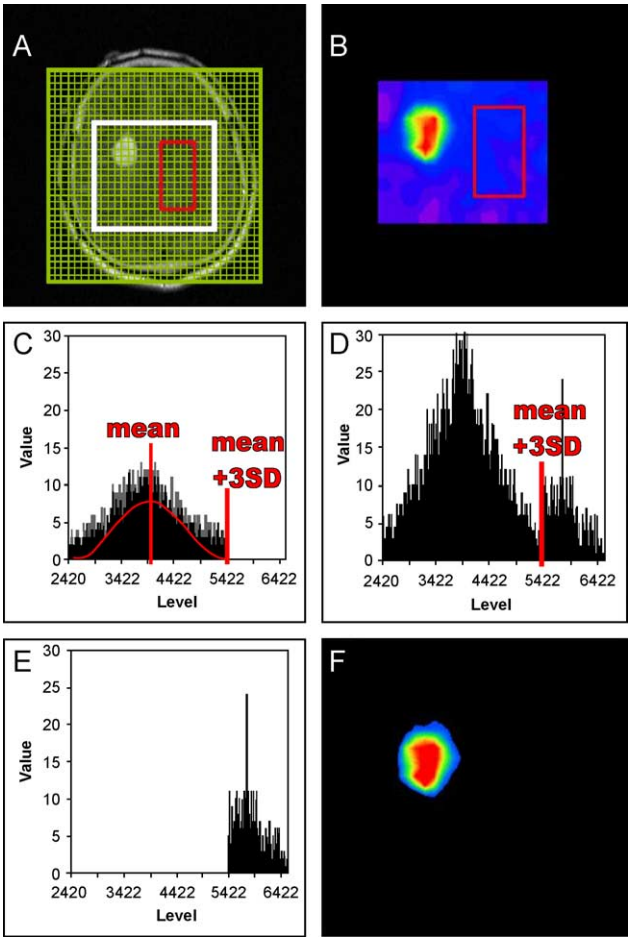

Fig. 2. Segmentation procedure (patient no. 5). (A) Anatomical reference (T2w) with CSI grid (green), VOI (white rectangle) and selected "healthy region" (red rectangle). (B) VOI-map of the Cho/NAA ratios with selected "healthy region" (red rectangle). (C) Histogram of the selected "healthy region" overlaid in red with the calculated Gaussian distribution and the mean and mean + 3SD of this histogram. (D) Histogram of the whole Cho/NAA map overlaid with the position of mean + 3SD cutoff calculated. (E) Histogram and (F) metabolic image of the segmented tumor. The FOV of the metabolic images (B) and (F) (including the black frame) corresponds to the CSI grid in (A). Color code: dark blue/violet, normal tissue; light blue/green, tumor border; and yellow/red: tumor center.

all Cho/NAA values in the whole map less than the mean + 3 SD were set to zero (Figs. 2D and E). This enabled the elimination of all but 0.3% of normal brain areas in the Cho/NAA map and hence the segmentation of the tumor (Fig. 2F). The segmentation procedure was tested with ^{1}H-MRSI data from healthy controls and a head phantom containing a physiological brain metabolite solution acquired with the identical measurement protocol described above.

MRI evaluation

The T2w TSE data set of the routine tumor MRI of each patient was contoured automatically using the medical imaging software OSIRIS (version 4.17) obtained from the University Hospital of Geneva, Switzerland (Paek et al., 2002). This segmentation strategy consists of a region growing algorithm starting with a seed point defined by both a neuroradiologist and neurosurgeon and growing a region by appending neighbors having similar gray levels. The results were subsequently reviewed and verified independently by an experienced neuroradiologist and a senior neurosurgeon in separate sessions. The T2w area was contoured as the area of hyperintensity on the TSE images. The maximum of the calculated T2w hyperintense areas covered by the PRESS-box delineated on the TSE images, corresponding to the MRSI slab, was used for comparison with the area of the segmented tumor in the Cho/NAA map.

Coregistration of metabolic and anatomical MR images

Accurate coregistration of the data of the MRSI slab (10 mm thick) with five slices (each 2 mm thick, no gap) of the anatomical MRI was achieved, due to having chosen the same FOV and precisely aligned the T1w SE protocol and the MRSI experiment. A combined data set consisting of MRI and MRSI data, a so-called MRI/MRSI hybrid data set, was created and matched exactly to a 3D data set for use with frameless stereotaxy (Stadlbauer et al., 2004).

Biopsy sampling and histopathological work up

Biopsy sampling was performed with the use of a frameless stereotactic system. Specimens were obtained from the region, which were defined according to the difference area between the metabolic map of the segmented tumor and the contoured T2w hyperintensity (Fig. 3A). The "difference area" is defined as the brain area which has abnormally high Cho/NAA but normal T2w signal. The location of the biopsy was labeled by the navigation software (Fig. 3B). Hence, the histopathological findings of the specimen could be tracked back to the actual voxel in the MR data set and, simultaneously, to the surgical site by video overlay.

All glioma specimens were histologically assessed according to the WHO classification of tumors of the nervous system. Tumor cells were identified using formalin-fixed and paraffin-embedded sections either stained with hematoxylin-eosin (HE) or monoclonal antibodies against p53, Map2c, or Ki67. Semiquantitative assessment of tumor cells versus preexisting brain parenchyma was obtained microscopically (Olympus, Hamburg, Germany) using analysis software (Analysis, Soft Imaging System GmbH, Leinfelden-Echterdingen, Germany) at 200-fold magnification in five different subfields of 348 × 261 μm in size. Only cells with a distinct nucleus were taken into account. All data were calculated as mean tumor cell number/whole cells in percent.

Results

Metabolic maps and segmentation

Our procedure for segmentation was tested with both MRSI data sets of the physiological metabolite solution in the brain phantom and the brains of controls. The Cho/NAA ratios of the selected regions were checked for Gaussian distribution for both controls and patients. All histograms showed an almost unimodal and symmetric distribution. In addition, the statistical test (David et al., 1954) confirmed the Gaussian nature of Cho/NAA ratio distribution. For the brain phantom, the three values differed by less than 1% and the area not removed after running the segmentation algorithm was less than 0.6% of the VOI. The

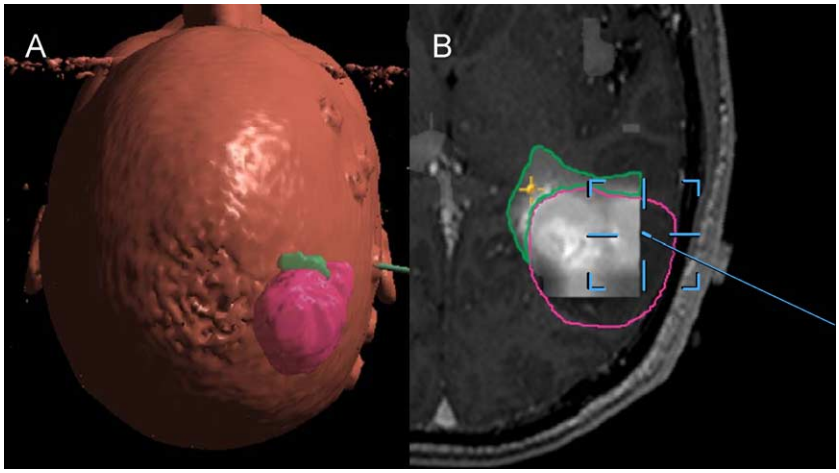

Fig. 3. Screenshots of the frameless stereotactic system software (patient no. 7). (A) 3D reconstructed biopsy sampling plan. The target volume was the difference volume (green) between the metabolic map of the segmented tumor and the contoured T2w hyperintensity (pink). (B) Enlarged axial slice with the location of the biopsy (yellow cross) in the difference volume labeled with the navigation software.

statistical evaluation of the ^{1}H-MRSI data of healthy controls showed that the differences in the three characteristic values for the selected regions of the control's brain were less than 1.7%. The residual area after segmentation of healthy brains was less than 3% of the VOI. Brain regions occasionally not removed were the ventricles and the sulci. The mean, median and modal value for the ratios in the selected normal brain region of patients differed by less than 3%. These results also confirmed our assumption of Gaussian distribution of the Cho/NAA ratios in normal brain.

Metabolic maps of Cho and NAA for a patient with an astrocytoma (WHO grade III) are presented in Figs. 1A and B. It is clear that the contrast tumor vs. normal brain in these images is not sufficient for delineation of the border zone of the tumor. The signal differences in the map of the Cho/NAA ratios (Fig. 1C) are more distinct and the region of tumor infiltration is more clearly visible than in Figs. 1A and B. Fig. 1D shows an anatomical reference of the same patient. The CSI grid and the PRESS preselected volume (white rectangle within the brain) are overlaid.

An anatomical reference with similar overlays of a patient with an oligoastrocytoma (WHO grade III) is presented in Fig. 2A. The selected "healthy region" is delineated as a red rectangle. The map of the Cho/NAA ratios calculated within the PRESS volume (Fig. 2B) demonstrates that the variation of the Cho/NAA values for normal brain are small and partial volume effects are reduced. The histograms of the selected region (red rectangle) and the whole Cho/NAA map are presented in Figs. 2C and D, respectively. The histogram and the resulting metabolic map after running the segmentation algorithm, that is, the spectroscopic image of the segmented tumor, are shown in Figs. 2E and F, respectively.

MRI/MRSI tumor area comparison and biopsy sampling

Our method for coregistration of MRI and MRSI data using a MRI/MRSI hybrid data set allows the direct comparison of T2w hyperintense areas and the areas of the segmented tumor in the Cho/NAA ratio map (Figs. 4B and E). Consequently, the fact that the PRESS selected region (PRESS box) did not always include the entire T2w hyperintense area was unproblematic. Furthermore, the frameless stereotactic software allowed tracking back the biopsy locations to the exact voxel position in the MR data set. For

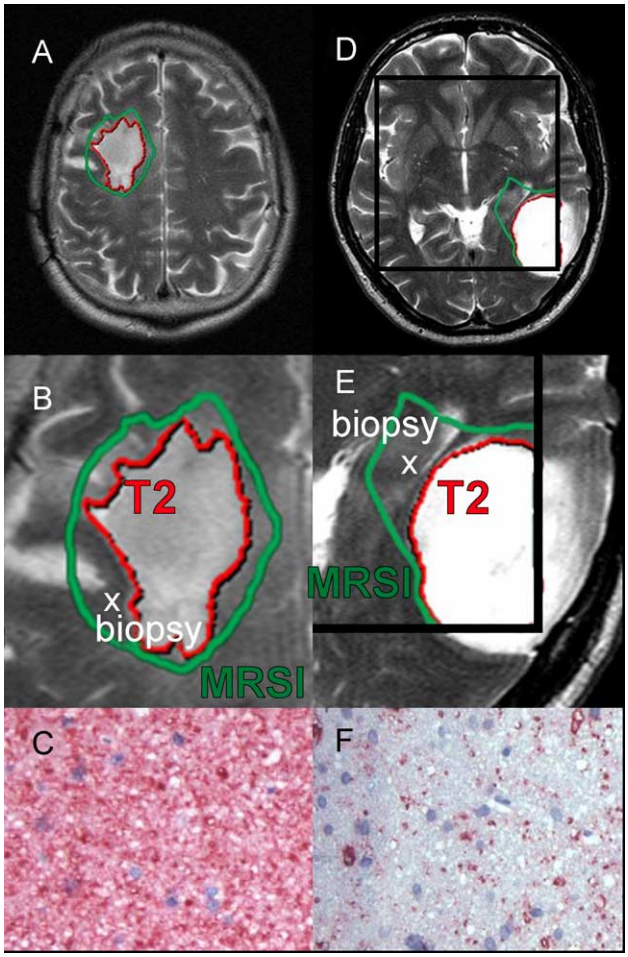

Fig. 4. Comparison of MRI/MRSI-defined tumor areas and biopsy sampling. (A and D) Anatomical images (T2w) of patients no. 5 and 7, respectively, overlaid with tumor border contours of the MRSI experiment (green) and T2w hyperintensity (red). The black rectangle delineates the position of the PRESS box. (B and E) Enlarged tumor images with the biopsy location (white cross). (C and F) Corresponding with 5% and 10% Map2c positive cells, respectively.

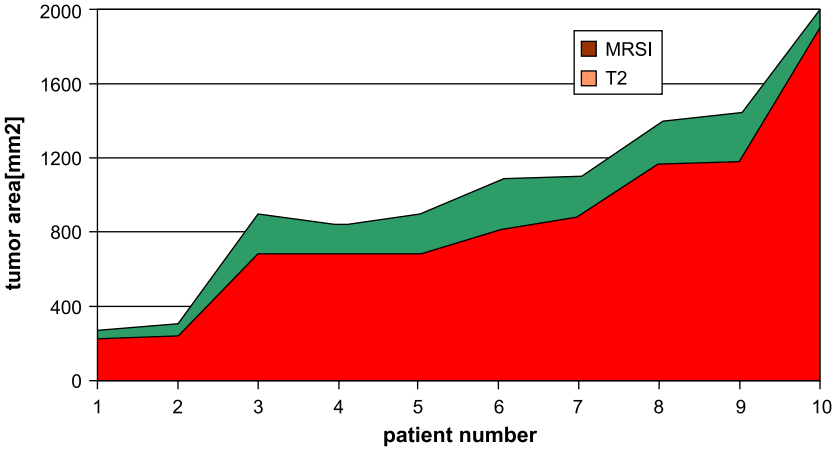

Fig. 5. Quantitative comparison of MRI/MRSI-defined tumor areas of all 10 patients. Tumor areas in the segmented Cho/NAA maps are shown in green and T2w hyperintense areas in red. Patients are ordered by increasing T2w hyperintensity just as in Table 1.

verification of the higher sensitivity in detection of pathologic changes of the MRSI experiment combined with the segmentation algorithm we used biopsies obtained from the area detected as tumor only by ^{1}H-MRSI (Fig. 3). In nine out of 10 patients biopsy sampling from a predefined area was successful. In one single case, a biopsy was impossible due to technical problems. In all nine cases histological findings showed tumor infiltration ranging from about 4–17% (mean 9%) of p53 or Map2c positive cells (e.g., Figs. 4C and F). All patients had segmented MRSI tumor areas that were greater than the T2w hyperintense areas covered by PRESS box (Fig. 5). The tumor areas according to the T2w hyperintensity ranged from 220 to 1902 mm^2, those according to MRSI ranged from 277 to 2017 mm^2. On average MRSI tumor areas were 24% larger compared to T2w areas (range 6–33%, $P = 0.00004$).

Discussion

^{1}H-MRSI has been used extensively for the evaluation of brain tumors. The major indications for brain tumor spectroscopy have ranged from differential diagnosis to assessment of treatment response. However, due to the lack of standardized methods for evaluation of multidimensional spectroscopic data, MRSI has not yet become a tool in clinical routine. Therefore, T2-weighted MRI, and pre- and postgadolinium contrast enhanced T1-weighted MRI are usually the basis for surgical or radiation therapy treatment planning of brain tumors. In an attempt to overcome these limitations, we developed an automated method for delineation and segmentation of the lesions related metabolic changes. We achieved significantly improved delineation for gliomas compared to the imaging strategies used in clinical routine. Furthermore, the delineated tumor borders were results of a mathematical process and not based on the investigator's experience.

It is known that the Cho/NAA ratio is markedly increased in brain neoplasms. We used maps of Cho/NAA ratios to achieve a better differentiation between normal brain and tumor tissue and also to reduce partial volume effects (McKnight et al., 2001). Investigation of normal brain regions of patients and healthy controls enabled us to establish the Cho/NAA ratio in normal brain tissue as being Gaussian distributed. The increased Cho/NAA ratio in tumor tissue and the Gaussian distribution in normal brain tissue were utilized to develop an algorithm for the differentiation of tumor tissue versus normal brain tissue. The result constitutes a novel method to segment gliomas on the basis of the biochemical changes by means of a user-independent algorithm. Comparison of the area of pathologic brain metabolism with the T2w hyperintense areas of routine MRI showed higher sensitivity in delineation of brain tumor borders. This was confirmed by histopathologic findings in the difference area between the MRSI and T2w hyperintensity tumor contours.

Our prime motivation was to improve the specificity of ^{1}H-MRSI in brain neoplasms by increasing spatial resolution and segmentation of the lesion specific changes in metabolism. Visualization of metabolic changes in brain tumors has been achieved via a number of approaches (Fulham et al., 1992; Go et al., 1995; Kamada et al., 2001; Mader et al., 1996; Preul et al., 1996). Images of different metabolite ratios (Cho/NAA, Cho/Cr and Cr/NAA) were utilized by Li et al. (2002) for evaluating and characterizing gliomas. De Edelenyi et al. (2000) showed six major metabolite peaks (Cho, Cr, NAA, alanine, lactate and/or lipids, and lipids) and information contained in T2-weighted MR images in a profile, so-called nosologic images, and used them for characterization of brain tumors.

As early as 1992, Fulham et al. showed that images for Cho and NAA are most suitable for tumor spectroscopy (Fulham et al., 1992). The signal differences between normal brain and tumor are sufficient to show the position of the tumor but not for accurate delineation of the border zone (Figs. 1A and B). In addition, partial volume effects of cerebrospinal fluid in sulci and ventricles modulate the level of these metabolites in normal brain tissue. This may cause metabolic variations in normal brain regions not related to pathology. In a recent publication McKnight et al. (2001) showed that the use of Cho/NAA ratios is suitable for delineation of the tumor border. They assumed that the relation between Cho and NAA in normal brain could be modeled as a linear function and used this to select voxels as internal controls for quantifying the probability of abnormality at each voxel location in patients with gliomas. In further studies of this group (Pirzkall et al., 2001, 2002), they achieved segmentation of brain tumors using this method and the definition of abnormality index contours. These contours and contours for T1w region of contrast enhancement and T2w region of hyperintensity were overlaid on anatomical images or on maps of Cho/NAA (Nelson et al., 2002) and used for target delineation in radiation therapy treatment planning. For low-grade

glioma they found that in 55% of their patients the MRSI contour was contained totally within the T2w contour. Furthermore, MRSI defined pathologic changes extending beyond the hyperintense T2w region was quite small and not distributed uniformly. For high-grade glioma they found that metabolically active tumor extended outside the hyperintense T2w region in 88% of their patients. Their findings were not validated by histology, however, and in contrast to their methods our approach is to segment the tumor in the metabolic image. This method reflects the pathology of the tumor in a more realistic way because tissue containing different levels of tumor infiltration is displayed according to its spatial distribution.

In conclusion, the method presented in our study utilizes the higher stability of metabolic ratios and a user-independent segmentation algorithm for delineation of brain tumors on the basis of the biochemical changes. We demonstrate that increasing spatial resolution MRSI in combination with our method can improve delineation of tumor borders compared the imaging routine clinical strategies. We have shown that ^{1}H-MRSI is more specific in the delineation of glial tumor cell infiltration than T2w signal changes. However, it is possible that p53 and Map 2c could be found beyond our calculation of tumor pathology based on metabolic changes determined by ^{1}H-MRSI. This may be due to the still rather course spatial resolution of our ^{1}H-MRSI experiment. To achieve even higher spatial resolution or increase the sensitivity it would be required to work at 3 T (Gruber et al., 2003) or higher field strengths not yet widely available in a clinical environment. Finally, the method presented has the potential for intraindividual and interindividual investigation of metabolic changes of other pathologies such as neurodegenerative disorders and epilepsy.

Acknowledgments

A.S. acknowledges financial support by the German Research Society (DFG Ga 638/2-1). S.G. acknowledges financial support by the Austrian Science Fund (FWF P14715-PSY). We thank S. Robinson for proofreading.

References

Croteau, D., Scarpace, L., Hearshen, D., Gutierrez, J., Fisher, J.L., Rock, J.P., Mikkelsen, T., 2001. Correlation between magnetic resonance spectroscopy imaging and image-guided biopsies: semiquantitative and qualitative histopathological analyses of patients with untreated glioma. Neurosurgery 49 (4), 823–829.

David, H.A., Hartley, H.O., Pearson, E.S., 1954. The distribution of the ratio, in a single normal sample, of range to standard deviation. Biometrika 41, 482–493.

De Edelenyi, F.S., Rubin, C., Esteve, F., Grand, S., Decorps, M., Lefournier, V., Le Bas, J.F., Remy, C., 2000. A new approach for analyzing proton magnetic resonance spectroscopic images of brain tumors: nosologic images. Nat. Med. 6 (11), 1287–1289.

Dowling, C., Bollen, A.W., Noworolski, S.M., McDermott, M.W., Barbaro, N.M., Day, M.R., Henry, R.G., Chang, S.M., Dillon, W.P., Nelson, S.J., Vigneron, D.B., 2001. Preoperative proton MR spectroscopic imaging of brain tumors: correlation with histopathologic analysis of resection specimens. Am. J. Neuroradiol. 22 (4), 604–612.

Frahm, J., Bruhn, H., Hanicke, W., Merboldt, K.D., Mursch, K., Markakis, E., 1991. Localized proton NMR spectroscopy of brain tumors using short-echo time STEAM sequences. J. Comput. Assist. Tomogr. 15 (6), 915–922.

Fulham, M.J., Bizzi, A., Dietz, M.J., Shih, H.H., Raman, R., Sobering, G.S., Frank, J.A., Dwyer, A.J., Alger, J.R., Di Chiro, G., 1992. Mapping of brain tumor metabolites with proton MR spectroscopic imaging: clinical relevance. Radiology 185 (3), 675–686.

Go, K.G., Kamman, R.L., Mooyaart, E.L., Heesters, M.A., Pruim, J., Vaalburg, W., Paans, A.M., 1995. Localised proton spectroscopy and spectroscopic imaging in cerebral gliomas, with comparison to positron emission tomography. Neuroradiology 37 (3), 198–206.

Gruber, S., Mlynarik, V., Moser, E., 2003. High-resolution 3D proton spectroscopic imaging of the human brain at 3 T: SNR issues and application for anatomy-matched voxel sizes. Magn. Reson. Med. 49, 299–306.

Jacobs, M.A., Horska, A., van Zijl, P.C., Barker, P.B., 2001. Quantitative proton MR spectroscopic imaging of normal human cerebellum and brain stem. Magn. Reson. Med. 46 (4), 699–705.

Kamada, K., Moller, M., Saguer, M., Ganslandt, O., Kaltenhauser, M., Kober, H., Vieth, J., 2001. A combined study of tumor-related brain lesions using MEG and proton MR spectroscopic imaging. J. Neurol. Sci. 186 (1–2), 13–21.

Kemp, G.J., 2000. Non-invasive methods for studying brain energy metabolism: what they show and what it means. Dev. Neurosci. 22 (5–6), 418–428.

Kondziolka, D., Lunsford, L.D., Martinez, A.J., 1993. Unreliability of contemporary neurodiagnostic imaging in evaluating suspected adult supratentorial (low-grade) astrocytoma. J. Neurosurg. 79 (4), 533–536.

Li, X., Lu, Y., Pirzkall, A., McKnight, T., Nelson, S.J., 2002. Analysis of the spatial characteristics of metabolic abnormalities in newly diagnosed glioma patients. J. Magn. Reson. Imaging 16 (3), 229–237.

Luyten, P.R., Marien, A.J., Heindel, W., van Gerwen, P.H., Herholz, K., den Hollander, J.A., Friedmann, G., Heiss, W.D., 1990. Metabolic imaging of patients with intracranial tumors: H-1 MR spectroscopic imaging and PET. Radiology 176 (3), 791–799.

Mader, I., Roser, W., Hagberg, G., Schneider, M., Sauter, R., Seelig, J., Radue, E.W., Steinbrich, W., 1996. Proton chemical shift imaging, metabolic maps, and single voxel spectroscopy of glial brain tumors. Magma 4 (2), 139–150.

Majos, C., Alonso, J., Aguilera, C., Serrallonga, M., Acebes, J.J., Arus, C., Gili, J., 2002. Adult primitive neuroectodermal tumor: proton MR spectroscopic findings with possible application for differential diagnosis. Radiology 225 (2), 556–566.

McKnight, T.R., Noworolski, S.M., Vigneron, D.B., Nelson, S.J., 2001. An automated technique for the quantitative assessment of 3D-MRSI data from patients with glioma. J. Magn. Reson. Imaging 13 (2), 167–177.

Michaelis, T., Merboldt, K.D., Bruhn, H., Hanicke, W., Frahm, J., 1993. Absolute concentrations of metabolites in the adult human brain in vivo: quantification of localized proton MR spectra. Radiology 187 (1), 219–227.

Miller, B.L., 1991. A review of chemical issues in 1H NMR spectroscopy: *N*-acetyl-L-aspartate, creatine and choline. NMR Biomed. 4 (2), 47–52.

Negendank, W.G., Sauter, R., Brown, T.R., Evelhoch, J.L., Falini, A., Gotsis, E.D., Heerschap, A., Kamada, K., Lee, B.C., Mengeot, M.M., Moser, E., Padavic-Shaller, K.A., Sanders, J.A., Spraggins, T.A., Stillman, A.E., Terwey, B., Vogl, T.J., Wicklow, K., Zimmerman, R.A., 1996. Proton magnetic resonance spectroscopy in patients with glial tumors: a multicenter study. J. Neurosurg. 84 (3), 449–458.

Nelson, S.J., Graves, E., Pirzkall, A., Li, X., Antiniw Chan, A., Vigneron, D.B., McKnight, T.R., 2002. In vivo molecular imaging for planning radiation therapy of gliomas: an application of 1H MRSI. J. Magn. Reson. Imaging 16 (4), 464–476.

Ott, D., Hennig, J., Ernst, T., 1993. Human brain tumors: assessment with in vivo proton MR spectroscopy. Radiology 186 (3), 745–752.

Paek, S.H., Kim, C.Y., Kim, Y.Y., Park, I.A., Kim, M.S., Kim, D.G., Jung, H.W., 2002. Correlation of clinical and biological parameters with peritumoral edema in meningioma. J. Neurooncol. 60 (3), 235–245.

Peeling, J., Sutherland, G., 1992. High-resolution 1H NMR spectroscopy studies of extracts of human cerebral neoplasms. Magn. Reson. Med. 24 (1), 123–136.

Pirzkall, A., McKnight, T.R., Graves, E.E., Carol, M.P., Sneed, P.K., Wara, W.W., Nelson, S.J., Verhey, L.J., Larson, D.A., 2001. MR-spectroscopy guided target delineation for high-grade gliomas. Int. J. Radiat. Oncol. Biol. Phys. 50 (4), 915–928.

Pirzkall, A., Nelson, S.J., McKnight, T.R., Takahashi, M.M., Li, X., Graves, E.E., Verhey, L.J., Wara, W.W., Larson, D.A., Sneed, P.K., 2002. Metabolic imaging of low-grade gliomas with three-dimensional magnetic resonance spectroscopy. Int. J. Radiat. Oncol. Biol. Phys. 53 (5), 1254–1264.

Preul, M.C., Caramanos, Z., Collins, D.L., Villemure, J.G., Leblanc, R., Olivier, A., Pokrupa, R., Arnold, D.L., 1996. Accurate, noninvasive diagnosis of human brain tumors by using proton magnetic resonance spectroscopy. Nat. Med. 2 (3), 323–325.

Steinmeier, R., Rachinger, J., Kaus, M., Ganslandt, O., Huk, W., Fahlbusch, R., 2000. Factors influencing the application accuracy of neuronavigation systems. Stereotact. Funct. Neurosurg. 75 (4), 188–202.

Stadlbauer, A., Moser, E., Gruber, S., Nimsky, C., Fahlbusch, R., Ganslandt, O., 2004. Integration of biochemical tumor images into frameless stereotaxy using a MRI/MRSI hybrid data set. J. Neurosurg. 101, 287–294.

Urenjak, J., Williams, S.R., Gadian, D.G., Noble, M., 1993. Proton nuclear magnetic resonance spectroscopy unambiguously identifies different neural cell types. J. Neurosci. 13 (3), 981–989.

van Der Veen, J.W., Weinberger, D.R., Tedeschi, G., Frank, J.A., Duyn, J.H., 2000. Proton MR spectroscopic imaging without water suppression. Radiology 217 (1), 296–300.

Vikhoff-Baaz, B., Starck, G., Ljungberg, M., Lagerstrand, K., Forssell-Aronsson, E., Ekholm, S., 2001. Effects of k-space filtering and image interpolation on image fidelity in (1)H MRSI. Magn. Reson. Imaging 19 (9), 1227–1234.